PHYSICAL REVIEW B **86**, 195315 (2012)

Temperature-dependent internal photoemission probe for band parameters

Yan-Feng Lao and A. G. Unil Perera[*]
Department of Physics and Astronomy, Georgia State University, Atlanta, Georgia 30303, USA
(Received 14 June 2012; revised manuscript received 15 October 2012; published 26 November 2012)

The temperature-dependent characteristic of band offsets at the heterojunction interface was studied by an internal photoemission (IPE) method. In contrast to the traditional Fowler method independent of the temperature (T), this method takes into account carrier thermalization and carrier/dopant-induced band-renormalization and band-tailing effects, and thus measures the band-offset parameter at different temperatures. Despite intensive studies in the past few decades, the T dependence of this key band parameter is still not well understood. Re-examining a p-type doped GaAs emitter/undoped $Al_xGa_{1-x}As$ barrier heterojunction system disclosed its previously ignored T dependency in the valence-band offset, with a variation up to $\sim -10^{-4}$ eV/K in order to accommodate the difference in the T-dependent band gaps between GaAs and AlGaAs. Through determining the Fermi energy level (E_f), IPE is able to distinguish the impurity (IB) and valence bands (VB) of extrinsic semiconductors. One important example is to determine E_f of dilute magnetic semiconductors such as GaMnAs, and to understand whether it is in the IB or VB.

DOI: 10.1103/PhysRevB.86.195315 PACS number(s): 73.40.Kp, 73.21.−b, 78.66.Fd

I. INTRODUCTION

Since its first application in lasers, the concept of heterostructure has become the basis of modern optoelectronics and high-speed microelectronics.[1] Among the most important aspects in a junction consisting of two dissimilar materials is its heterointerface at which differences in band gaps give rise to a band offset across the interface. Offering the possibility of designing confinements for electrons/holes and photons, the band offsets are determinative for the characteristics of semiconductor heterojunction based devices. Given its significance, it was not surprising that this parameter was studied by numerous methods,[2–4] still without overall agreement. With respect to heterojunctions where experimental data are unavailable, the common practice is to use the model-solid theory.[5] Throughout the literature, band offsets were generally taken to be temperature (T) independent, based on the assumption that band gaps of heterojunction constituents have equal temperature coefficients,[6] or probably owing to the lack of a general study on the T dependency.[7,8] Here, we report a method that can measure the T variations of band offsets. The temperature coefficients of the valence-band offsets were determined for $GaAs/Al_xGa_{1-x}As$ heterojunctions, which were usually believed to have constant offset values over temperatures.

The band offsets can be expressed by $\Delta E_{c(v)} = \Delta E_{c(v),0} + \Delta V$, where $\Delta E_{c(v)}$ is the offset between the conduction (valence) bands [CBs (VBs)] of two semiconductors in a heterojunction. $\Delta E_{c(v)}$ consists of two contributions: $\Delta E_{c(v),0}$, which is a quantity describing the bulk properties of semiconductors, and ΔV, the electrostatic potential lineup[9] of the junction. ΔV results from the local reconstruction of atomic and electronic structure at the heterointerface. As ΔV is trivial for lattice-matched isovalent heterojunctions such as GaAs/AlGaAs,[10] the T dependence of band offsets can be identified from the difference in band gaps ($\Delta E_g^T \equiv \Delta E_{c,0}^T + \Delta E_{v,0}^T$) between heterojunction constituents and using tabulated band-gap parameters.[6,7] One of the examples is the mercury cadmium telluride (MCT) junction. Owing to the opposite T variations of band gaps between HgTe and CdTe, ΔE_g shows appreciable dependence on the temperature. However, controversial observations with opposite trends of the T dependence still exist.[11] Based on photoluminescence (PL) measurements and fittings, Becker *et al.*[11] obtained a negative temperature coefficient of ΔE_v^T. Their results are contrary to earlier reports[11,12] with increased ΔE_v at high temperatures. According to the band-gap parameters,[13] the band offsets should decrease with temperature, thus justifying the T-dependent trend obtained by Becker *et al.* Nevertheless, further studies on heterojunctions consisting of $Hg_{1-x}Cd_xTe/Hg_{1-y}Cd_yTe$ could confirm this trend improving MCT-based infrared device designs.

By analyzing external photoemission experiments, Fowler[14] initially indicated possible T dependence of the work function. In terms of the electron affinity rule or the model-solid theory,[5] the band offset should vary with temperature accordingly. In addition, attention should be given to the band-offset T dependency of heterovalent junctions, which are composed of semiconductors from different columns of the periodic table.[15] The localized electric dipoles due to net interface charge[8] strongly depends on the temperature and thus takes a critical role in the T dependence of band offsets.

In this paper, using temperature-dependent internal photoemission spectroscopy (TDIPS), we show (i) the evidence of T dependency in band offsets, (ii) the finding of previously ignored offset variation with temperatures for $GaAs/Al_xGa_{1-x}As$, and (iii) the study of electronic structure of extrinsic semiconductors, such as the Fermi energy level (E_f), band-gap renormalization (BGR)[16] and band tailing.[17] This method is helpful to understanding the presently debated electronic structure of diluted magnetic semiconductor (DMS) (Ga,Mn)As, whether the E_f lies in the impurity[18–20] or valence[21,22] band (IB or VB). The method reported here is analogous to external photoemission.[14] However, with the emission of carriers over a barrier rather than into the vacuum, TDIPS can give a measure of the internal work function or photoemission threshold (labeled as Δ) and determine the band offsets at the heterointerface. The band offsets decreasing

 ©2012 American Physical Society

with the temperature with a variation up to $\sim\!-10^{-4}$ eV/K was observed in the GaAs/AlGaAs system, which should have an effect on the operation of devices in the THz range. Two important infrared material systems of InAs/GaSb and $Hg_{1-x}Cd_xTe/Hg_{1-y}Cd_yTe$ have the prominent T dependence of band offsets by comparing with $GaAs/Al_xGa_{1-x}As$, and so do the hybrid photonic heterostructures[23] such as III-V/Si. The T-dependent characteristic would suggest new strategies in designing devices using these semiconductor systems.

In the next section, the theoretical basis of the TDIPS methodology is presented. Section III describes the experimental details and results. TDIPS distinguishing the IB and VB of p-type semiconductors is discussed in Sec. III A to show an accurate determination of Δ as a function of E_f. In Sec. III B, the TDIPS method is also used to reappraise the IPE data of an n-type GaAs/AlGaAs junction reported by Coluzza *et al.*[3] and compared with their results based on the Fowler method.[14] Based on the demonstrated accuracy of TDIPS, we obtain the band offsets of p-type $GaAs/Al_xGa_{1-x}As$ heterojunctions and their T dependence. Section IV discusses the TDIPS analysis and advantages of using p-type junctions for internal photoemission (IPE) measurements. We conclude in Sec. V.

II. TEMPERATURE-DEPENDENT INTERNAL PHOTOEMISSION ANALYSIS

The IPE spectroscopy is an attractive method for studying heterojunctions. Based on the common characteristics in the generation and emission of photocarriers across a heterointerface, IPE exists in the optical processes of bulk,[24] quantum,[25] and even semiconductor-liquid electrolyte junctions.[26] The IPE signal can be detected through an electric field,[24] a second photon,[27] or second-harmonic generation.[28]

The theoretical basis of IPE can be traced back to Fowler's works[14] on external photoemission of electrons from metal to vacuum. Originally, Fowler derived a photoemission yield function containing T-dependent terms, expressed by

$$Y \sim (kT)^2 f(\mu), \tag{1}$$

where Y denotes the quantum yield, defined as the number of emitted carriers per one absorbed photon. $f(\mu)$ is defined as,[14]

$$f(\mu) = \begin{cases} e^{\mu} - e^{2\mu}/4 + e^{3\mu}/9 - \cdots & (\mu \leqslant 0) \\ \pi^2/6 + \mu^2/2 - (e^{-\mu} - e^{-2\mu}/4 + e^{-3\mu}/9 - \cdots) & (\mu \geqslant 0) \end{cases} \tag{2}$$

in which $\mu \equiv (h\nu - \Delta)/kT$ and $h\nu$ is the photon energy. Other symbols have their usual meanings. Fowler's yield function can be actually reduced[29] to a T-independent form for $h\nu > \Delta + 3kT$, i.e.,

$$Y(h\nu) \sim (h\nu - \Delta)^2. \tag{3}$$

In spite of its original derivation for external photoemission the Fowler's yield function was applied[3] to many IPE cases; particularly, the T-independent yield expression [Eq. (3)] was adopted. To account for the difference in the electronic structures between semiconductors and metals, replacing the exponent "2" in Eq. (3) with a constant p was proposed.[30–33] Typically, p varies from 1–3.[33] In spite of acceptable fittings by using best-fit values of p, the meaning of such a yield function is obscure, and importantly its independence on temperature leads to underestimated Δ values. Such underestimation is more significant in semiconductor junctions where Δ is much less than 1 eV.

The operating principle of TDIPS is depicted in Fig. 1(a) in which two doping cases with E_f lying (i) above and (ii) below the VB edge are schematically shown. Here, photoemission occurs by following one-photon excitation. High-energetic holes originating from states around E_f by absorbing photons are injected into the VB of the barrier. Typical photoemission processes [labeled as (1) and (2)] include optical transitions and the escaping of holes. Shown in the inset of Fig. 1(a) are the schematic transfers of carriers from the VB of the emitter to the VB of the barrier. This may include photon absorption and scattering events, which direct the excited holes passing over the interface and injecting into the barrier. The holes in the emitter can be optically excited through both direct and indirect transitions. However, the transitions that provide the majority contribution to the quantum yield would rely on the incident photon energy. For the near-threshold regime, holes must end up at states near the edge of the potential barrier in order to escape over the heterointerface; hence, indirect transitions have a higher probability to occur. When the photon energy is greater than the threshold, photoexcited holes from direct transitions, which end up at higher energy states of the VBs, are capable of escaping over the barrier. This leads to the majority contribution to yield by direct transitions,

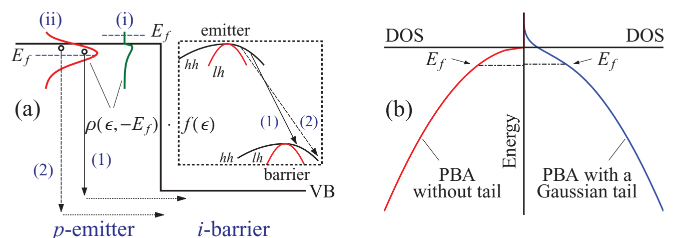

FIG. 1. (Color online) (a) The VB diagram of a p-emitter/i-barrier IPE system. $\rho(\epsilon,-E_f)f(\epsilon)$ is the multiplication of the hole energy distribution (ρ) and the FD function (f). Shown are the (i) nondegenerate and (ii) degenerate doped emitter. Typical IPE processes are labeled as (1) and (2), consisting of optical transitions in the emitter and the escaping of holes from the VB of the emitter to the VB of the barrier. (b) Schematic DOS as a function of energy. By including a band tail, hole states are extended into the forbidden gap (atop the VB). The DOS tail contributes a higher photoemission yield at $h\nu > E_f + \Delta$ compared to that without the DOS tail.

because direct transitions have much higher transition rates than indirect transitions. In the present study, both direct and indirect transitions are taken into account.

As for the determination of band offsets, the most important factor is to account for the spectral line shape of the quantum yield. Therefore, the consideration of dominant processes affecting the energy distribution of carriers and their escape probabilities across the interface will be sufficient. By taking into account the photoexcitation of holes in the emitter through inter-valence-band (IVB) transitions,[34] described by an energy distribution function $\rho(\epsilon, h\nu - E_f)$, and the transmission of holes over the barrier, described by a probability function of $P(\epsilon, \Delta)$,[35] the quantum yield reads

$$Y(h\nu) = Y_0(kT) + C_0 \int_{\Delta}^{\infty} \rho(\epsilon, h\nu - E_f)\, f(\epsilon, h\nu)\, P(\epsilon, \Delta)\, d\epsilon, \tag{4}$$

where C_0 is a constant independent of ϵ and $h\nu$. ϵ is the energy of photoexcited holes. Δ is defined as the energy difference between the Fermi level and the VB edge of the barrier. The energy is scaled downward with the zero reference at the Fermi level. Equation (4) describes the case of degenerate (highly) doped emitters (E_f lying within the VB), and can adapt to the nondegenerate doping case by changing the sign of E_f. At finite temperatures, carriers occupy energy states above the Fermi level in terms of the Fermi-Dirac (FD) statistics. An FD-like function $f(\epsilon, h\nu) = [1 + e^{(\epsilon - h\nu)/kT}]^{-1}$ was used as the distribution function. This is based on an assumption that photoexcited holes remain in the same distribution as that before photoexcitation, with the only difference in energy by $h\nu$.

As a result of the FD distribution, holes with energies greater than Δ can escape without the need of absorbing incident photons, leading to a thermionic emission term Y_0 included in Eq. (4). The photocurrent measurements[35] typically need to separate the thermionic emission component from the photoemission yield, and hence require accurate knowledge of the sample temperature which could vary due to light absorption. As suggested by Williams,[35] the true origin of the observed currents, either due to photoemission or thermionic emission, can be resolved by taking spectral measurements, since the thermionic emission current is independent of the photon energy and only gives a constant background signal. By setting Y_0 to the experimental yield value at the spectral range far below Δ, the thermionic emission background can be distinguished from the yield spectra, allowing for a fitting to the photoemission yield component alone. In addition, a calibration of the sample temperature may be required if absorption of infrared light causes appreciable temperature variations in the sample. However, such a variation is negligible in our experiment, as our temperature controller typically has the stabilization accuracy of $< \pm 0.1$K.

The transmission of photocarriers passing through the heterointerface is described by a probability function of $P(\epsilon, \Delta)$, taken as $\sim(\epsilon - \Delta)$ for $\epsilon \geqslant \Delta$ and 0 for $\epsilon < \Delta$. This results from the escape cone model where carriers are capable of escaping over a barrier by having the normal (to the interface) momentum greater than that of the potential barrier. These carriers occupy energy states on a spherical Fermi cap in the $\boldsymbol{k}$ space.[35,36]

The spectral line shape of the quantum yield is primarily determined by the energy distribution $[\rho(\epsilon, \epsilon_0)]$ of photocarriers in the emitter. As direct transitions associate with the joint density of states (JDOS) and indirect transitions in a limited photon-energy range (e.g., the near-threshold regime with final states near the Γ point of the barrier) are mainly determined by the occupation of initial states,[37] $\rho(\epsilon, \epsilon_0)$ approximates to taking the density of states (DOS) line shape of the VB. Therefore, the direct and indirect transitions actually lead to the same energy dependency. For optical transitions occurring around the Γ point, the parabolic-band approximation (PBA) is taken, giving $\rho(\epsilon, \epsilon_0) \sim (\epsilon - \epsilon_0)^{1/2}$.

As a result of doping into emitters, the IPE model should also handle dopants-caused effects such as the band tail. Dopants introduce potential fluctuations and a band tail atop the VB. The PBA DOS is thus modified in terms of the Kane model,[38] as shown in Fig. 1(b). Dopants-perturbed DOS mainly changes the near-threshold line shape of the quantum yield, by increasing the yield for $h\nu > E_f + \Delta$ due to optical transitions from the extended states in the forbidden gap, and slightly reducing the yield for $h\nu < E_f + \Delta$. This results in smaller Δ extracted from fittings to yield spectra, compared to that using the unperturbed DOS. Influence of the band tailing on E_f is believed to be negligible.[39]

Another possible influence on the IPE yield could be from the difference in effective masses between the emitter and barrier. This was previously discussed by Chen *et al.*[40] They obtained a yield function containing effective masses based on interband transitions from VB to CB. The dependence of IPE yield on the difference of effective masses (or the Al fraction of $Al_xGa_{1-x}As$ barrier for a $GaAs/Al_xGa_{1-x}As$ structure) can be understood by fitting the yield data calculated from[40] the yield function of Chen *et al.* using a power-law function (i.e., $Y \propto \epsilon^{\gamma}$) where ϵ is defined[40] as $(h\nu - E_T)/q\phi_B$ with E_T and $q\phi_B$ the threshold energy and barrier height, respectively. It turns out that γ varies from 1.97 to 2.31 when x changes from 0.1 to 0.6. Such a variation of γ does not result in a significant change in the threshold energy being fitted. For example, Coluzza *et al.*[3] obtained a threshold energy of 0.218 eV for an n-type GaAs/AlGaAs structure by fitting to the yield spectrum with a square power law yield function ($\gamma = 2$). For the fittings with γ varying from 1.97 to 2.31, the threshold energy varies from 0.216 to 0.220 eV. This indicates that the influence of the variation in the γ due to effective mass mismatch on the threshold is less than 1% and hence negligible. Chen *et al.*[40] also predicted an effective-mass-dependent crossover on the yield spectra where the variation of yield with the photon energy starts to change. They also indicated that such a crossover was experimentally observed in the IPE experiment reported by Coluzza *et al.*[3] in the interband photon energy range ($>$1.6 eV). However, the crossover ($=\epsilon_{\mathrm{tr}} q\phi_{\mathrm{B}} + E_T$, where ϵ_{tr} is a parameter)[40] occurs at an energy typically greater than the near-threshold regime where yield analysis was carried out in order to determine the threshold energy. Based on the above reasoning, the effect of mismatch in the effective masses between the emitter and barrier on determining the threshold energy will be insignificant. In our analysis, the DOS of the emitter and transmission probability of holes across the heterointerface are related to the effective masses of holes, which only appear in the constant term of C_0 in Eq. (4). We

specifically applied the IPE analysis based on Eq. (4) to the intra-band transition range (<0.3 eV) of the data of Coluzza *et al.*[3] to reinspect the ΔE_c value. The details are discussed in Sec. III B1.

In order to compare with the Fowler's formalism [Eq. (3)], an analytical form of Eq. (4) was deduced for $h\nu > \Delta + E_f$ by neglecting the band tailing, i.e.,

$$Y(h\nu) \sim Y_0'(E_f,kT) + \phi(E_f)[h\nu - \Delta - (2/5)E_f] + \psi(E_f,kT)[h\nu - \Delta - E_f + (3/2)kT], \quad (5)$$

where Y_0', ϕ and ψ only rely on variables in the brackets. This clearly accounts for the dependence of quantum yield on E_f and T. In order to properly extract Δ, the influences of E_f and T have to be taken into account, particularly at high temperatures. Also, Eq. (5) predicts the linear spectral line shape instead of the Fowler-like power-law yield function.

III. EXPERIMENTAL DETAILS AND TDIPS RESULTS

The semiconductor heterostructures used in this study are based on GaAs/$Al_xGa_{1-x}As$ material systems, consisting of multiple periods of p-type GaAs emitters and undoped $Al_xGa_{1-x}As$ barriers grown by molecular-beam epitaxy (MBE). The periodic region was sandwiched between top and bottom (p^+-GaAs) ohmic contact layers. Detail structure parameters are listed in Table I. Samples were processed by wet etching to produce square mesas, followed by Ti/Pt/Au ohmic contacts evaporated onto the top and bottom contact layers. A top ring contact with a window opened in the center was used to allow for front-side illumination. Samples were mounted in a Dewar with varied temperature from the temperature of liquid helium or nitrogen up to room temperature (RT) by using a built-in heater. The photocurrent spectra were measured on samples with active area of $260 \times 260 \sim 660 \times 660\ \mu m^2$ by using a Perkin-Elmer system 2000 Fourier transform infrared (FTIR) spectrometer. In order to eliminate the influence of light source and optical components on the spectral line shape, the background signal was recorded by using a commercial bolometer, which has the flat sensitivity over the entire wavelength range being measured.

The quantum yield is proportional to the multiplication of spectral responsivity[34] and photon energy. To obtain the photoemission threshold (Δ), fittings to the yield spectra were carried out in the near-threshold regime by using Eq. (4) and the Levenberg-Marquardt fitting algorithm. Y_0, C_0, and Δ are regarded as fitting parameters. E_f was determined by carrying out an 8×8 $\boldsymbol{k} \cdot \boldsymbol{p}$ computation[41] and integrating the product of DOS by the FD distribution function over the entire range of energies. The upper end of the fitting range is near the point at which the yield line shape starts to change, while the lower end is selected at the spectral regime, which has the higher intensity than the noise level. However, the fitting results are insensitive to the selection of the fitting range. At high temperatures, a nonzero thermionic emission current mixes into the yield spectrum. In this case, Y_0 of Eq. (4) is set to the experimental yield value at the $h\nu \to 0$ (eV) limit.

TABLE I. GaAs/$Al_xGa_{1-x}As$ heterojunction parameters. All samples have the same emitter thickness of 18.8 nm. Δ_{BGR} is the band-gap renormalization (BGR-) caused VB shifting and calculated according to Ref. 43.

Sample No.	Al mole fraction x	Barrier thickness (nm)	Emitter doping (cm^{-3})	Periodic numbers	Δ_{BGR} [Cal.] (meV)
S12a	0.12	125	1×10^{17}	16	6
S12b	0.12	125	1×10^{18}	16	13
S15	0.15	125	3×10^{18}	12	20
S28	0.28	60	3×10^{18}	30	20
S37	0.37	60	3×10^{18}	30	20
S57	0.57	60	3×10^{18}	30	20

A. Distinguishing the IB and VB by TDIPS

In this section, TDIPS is used to distinguish the IB and VB of extrinsic semiconductors at different doping densities. This investigation would be useful for studying (Ga,Mn)As which is presently under debate about its electronic structure. In particular, for hole density higher than the insulator-to-metal transition (IMT) density,[18] hole transport in (Ga,Mn)As is debated to be through the IB[18–20] or VB.[21,22] Ideally, quantum yield depends in part on the multiplication of the energy distribution function $[\rho(\epsilon,-E_f)]$ related to the band structure and the FD distribution function $[f(\epsilon)]$, which represents the available number of carriers for photoemission. It is thus anticipated that TDIPS is sensitive to the band parameters, particularly to E_f. Two cases of doping densities with different E_f and $[\rho(\epsilon,-E_f)f(\epsilon)]$ are schematically shown in Fig. 1(a).

The dopant-induced energy level typically undergoes the following evolutions as the doping density increases: i) expansion into an IB and start to mix with the VB (not yet merged; the so-called separate-band picture or IB conduction); and ii) IB merged with the VB where carriers have the zero activation energy (the merged-band picture or VB conduction). The present study demonstrates TDIPS clarification between the band pictures of p-type emitters in GaAs/AlGaAs junctions doped to $1 \times 10^{17}\ cm^{-3}$ [sample S12a, the separate-band picture][18] and $1 \times 10^{18}\ cm^{-3}$ [sample S12b, the merged-band picture],[42] respectively. Their photoemission thresholds satisfy $\Delta_a - \Delta_b = (E_{f_b} - E_{f_a}) + (\delta_{BGR} - \delta_{\phi_i})$, as shown in the inset of Fig. 2(a). $\delta_{BGR}(-7\ meV)$ and $\delta_{\phi_i}(-8\ meV)$ are the difference of the BGR-caused VB shifts (Δ_{BGR})[43] between S12a and S12b, and the difference of the multiple-image force (MIF) barrier lowerings $(\Delta\phi_i)$,[44] respectively. The bias-dependent MIF lowering can be evaluated by considering two emitters beside a barrier.[44]

When the photon energy is much less than Δ, ideally holes are unable to escape out of the emitter by absorbing photons. The yield spectrum of S12b shown in Fig. 2(a) approaches a horizontal shape when the photon energy goes below Δ, and its yield approaches a nonzero value, which equals Y_0 of Eq. (4). On the contrary, the yield of S12a approaches the value (when $h\nu \to 0$ eV) much less than that of S12b. This implies a higher Δ value of S12a than that of S12b, since the thermionic emission current exponentially varies with Δ.

IVB absorption[34] is proportional to the hole density and partially interprets the quantum yield of sample S12b higher than that of S12a as shown in Fig. 2(a). However, their yield difference is due mainly to the difference of $[\rho(\epsilon,-E_f)f(\epsilon)]$

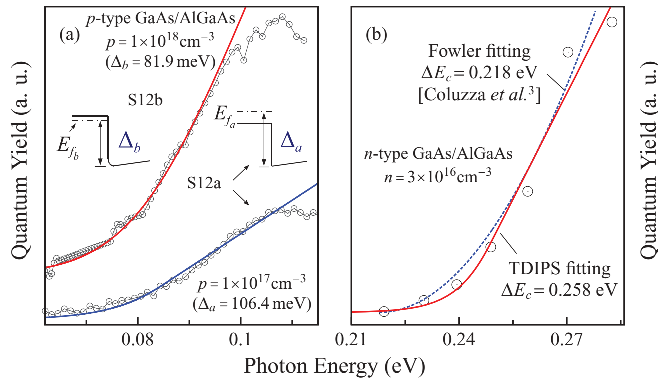

FIG. 2. (Color online) (a) TDIPS fittings to the quantum yield spectra of samples S12a and S12b the emitters of which are nondegenerate and degenerate doped, respectively. The higher yield of S12b at the low-energy end than S12a results from the thermionic emission. Their Fermi level difference was obtained to be $E_{f_b} - E_{f_a} = 24.5$ meV. The corresponding band pictures with E_f lying in the band gap (S12a) and in the VB (S12b) are shown in the insets. The different sharpnesses of barriers close to the heterointerface are due to the MIF barrier lowerings. (b) TDIPS fitting (solid line) to the IPE data (scattered data points) of the n-type GaAs/Al_xGa_{1-x}As heterojunction adopted from Coluzza *et al.*,[3] along with the comparison with their Fowler fitting[14] (dashed line).

between these two samples, pointing to the varied E_f. The fitted Δ_a and Δ_b are 106.4 meV and 81.9 meV, respectively, giving rise to $E_{f_b} - E_{f_a} = 24.5$ meV, which is close to Be (p-type dopant) binding energy (28 meV).[18] Since the behaviors of dopants in GaAs are well known, we calculated E_f in order to compare with fitted results. Based on the insulating behavior[18] of p-type GaAs of sample S12a, its E_{f_a} was calculated to be -21.6 meV, thus giving $E_{f_b} = 2.9$ meV. This agrees with the calculated value of 1.5 meV based on the merged-band picture of 1×10^{18} cm^{-3} p-type doped GaAs.[42]

In general, E_f can be obtained through measuring samples with different doping densities. Impurities in semiconductors usually have the known binding energies. For example, the magnetic dopant of Mn in GaAs has a larger binding energy ($\sim$0.112 eV) than that of the nonmagnetic dopant of Be.[18] By measuring samples with varied doped densities, Δ at the dilute doping where E_f approaches the binding energy can be deduced. This determines ΔE_v since $\Delta = |E_f| + \Delta E_v$ for the dilute doping case. The obtained ΔE_v in turn determines E_f of samples with different doping densities, thus identifying the separate- or merged-band pictures.

The above analysis revealed two important characteristics of TDIPS: (i) determining Δ precisely, thus capable of sensing a minute T variation, and (ii) distinguishing band structures with IB and VB separated or merged.

B. Determination of band offsets and their T dependence

Based on demonstrated accuracy, TDIPS is used to measure the band offsets and determines possible T dependency. The GaAs/AlGaAs heterojunctions have been studied.

1. *n-type GaAs/AlGaAs heterojunctions*

In this section, TDIPS is applied to reappraising the IPE data of Coluzza *et al.*[3] (n-type GaAs/Al_xGa_{1-x}As) and compared with their results based on the Fowler fitting method.[14] Coluzza *et al.*[3] reported the conduction band offset (ΔE_c) of n-type ($n = 3 \times 10^{16}$ cm^{-3}) GaAs/Al_xGa_{1-x}As heterojunctions by IPE measurements with the Vanderbilt free-electron laser as the optical source. They used the Fowler's yield function[14] of Eq. (3) to fit the near-threshold regime, as shown in Fig. 2(b), which gives ΔE_c of 0.218 eV. In terms of the relationship between ΔE_c and x reported by O'Shea *et al.*:[2] $\Delta E_c = 0.84\,x$ (eV) where ΔE_c varies between 0.21 – 0.23 eV by taking into account experimental uncertainties,[3] the equivalent Al fraction is $x = 0.25 - 0.27$, which is, however, less than their photoluminescence (PL) determined value of $x = 0.30$. They ascribed this difference to the changes in the stoichiometry of MBE grown Al_xGa_{1-x}As on going from the bulk ($x = 0.3$) to the region immediately close to the interface ($x = 0.2$). This would result in a potential grading in the barrier around the GaAs/AlGaAs interface. Thus, electrons should see a varied barrier height due to the barrier tilting under applied bias. However, such observations were not identified in their experiments.

As discussed in Sec. II, Δ is typically underestimated by the Fowler method. With increasing the temperature, the Fermi level shifts deep into the band gap, whereas the higher-energy states of the CB will be more populated by electrons. This results in the shift of the near-threshold yield edge toward the lower photon energy end. Such temperature-related effects have to be taken into account in the quantum yield expression, in order to properly extract Δ. To apply our TDIPS model [Eq. (4)] to the nondegenerate case,[3] we set E_f to -9 meV. Here, the negative sign of E_f means the Fermi level lying below CB. The fitting shown in Fig. 2(b) gives the $\Delta E_c \sim 0.258$ eV or $x \sim 0.307$, which is consistent with the PL result of Coluzza *et al.*,[3] and also indicates the accuracy of the TDIPS analysis.

2. *p-type GaAs/AlGaAs heterojunctions*

The VB offsets of GaAs/Al_xGa_{1-x}As heterojunctions (Table I) and their T dependence were obtained through analyzing quantum yield spectra at different temperatures, as shown in Figs. 3(a)–3(d). Originating from IVB transitions, the IPE spectra can show characteristics related to the VB structure[34] such as the spin-orbit split-off band and heavy-hole band (*so-hh*) splitting. By comparing with direct transitions, indirect transitions could have the majority contribution to the IPE yield in the near-threshold regime. This is in contrast to absorption measurement dominated with the direct transitions, and may provide experimental evidence for phonon-assisted IVB absorption.[45]

To reduce the uncertainty related to the calculation of MIF barrier lowering $\Delta\phi_i$, Δ is extrapolated at zero bias voltage, as shown in Fig. 4(a) where typical plots of Δ against (Electric Field)$^{1/2}$ are shown. The linear variations of Δ with (Electric Field)$^{1/2}$ confirm the MIF effects. The VB offsets were then obtained by $\Delta E_v = \Delta - \Delta_{\rm BGR} + E_f + \Delta\phi_i$. In order to compare with previous reported T-independent values (Table II),[2,7] the ΔE_v data were averaged over various

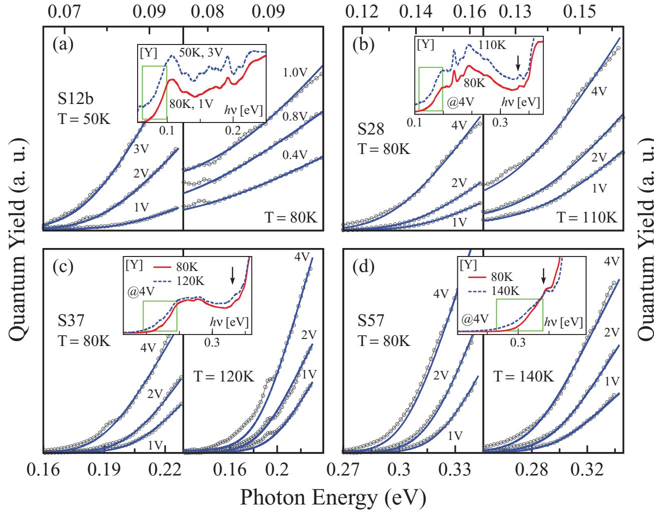

FIG. 3. (Color online) (a)–(d) are typical experimental quantum yield spectra (scattered data) of GaAs/$Al_xGa_{1-x}As$ heterojunctions (see Table I for sample structures) at different bias voltages and temperatures. Solid lines are the TDIPS fitting curves based on Eq. (4) with Y_0, C_0 and Δ as the fitting parameters. The thermionic emission yield (Y_0) increases with increasing biases and temperatures. Insets plot the yield spectra in a larger energy range to show the IVB transitions where arrows indicate the *so-hh* onsets. The rectangle frames indicate the regions where fittings were made.

temperatures and fitted by a linear dependence of ΔE_v on the Al mole fraction, as shown in Fig. 4(b). Our result agrees well with the data of Batey *et al.*[2] obtained from the Arrhenius plots over the temperature range from ~80 K to RT, and is in the middle of the 4.2 K data of Yi *et al.*[2] and the RT data of Vurgaftman *et al.* for GaAs/AlAs.[7] To reconcile the slight difference between different temperatures, ΔE_v has to vary with temperature. This can be seen from the plots of TDIPS data at different temperatures as shown in Fig. 5(a). The temperature coefficients of ΔE_v^T are thus fitted, where recent reported data at 4.2 K by Yi *et al.*[2] were taken into account. This also results in T-dependent ΔE_v as a function of Al mole fraction: $\Delta E_v = (0.570 - 1.39 \times 10^{-4}\ T)x$ (eV). The band offset can also be described by the offset ratio of $r = \Delta E_c : \Delta E_v$. Taking into account the T variations, r varies from 59 : 41 at 4.2 K[2] to 61 : 39 at 300 K for $x = 0.4$. The latter value is close to 62 : 38 suggested by Kroemer.[1] It is also clear that $\Delta E_v = 0.59$ eV of GaAs/AlAs predicted by the first-principles calculations and model-solid theory[5,7] is more close to the offset value at the $T \rightarrow 0$ K limit.

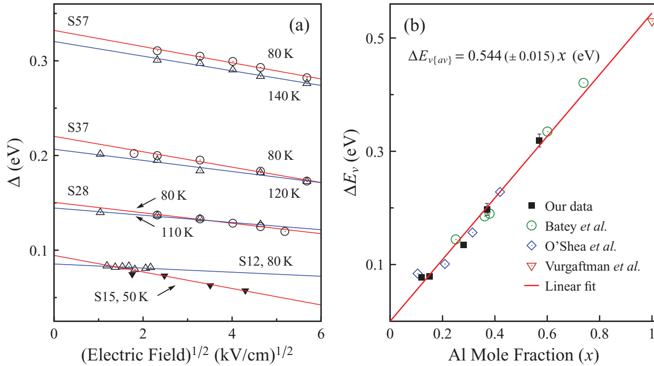

FIG. 4. (Color online) (a) Typical plots of Δ against (Electric Field)$^{1/2}$. Solid lines are the least-square fits according to the relationship between the MIF barrier lowering and the electric field. Extrapolated Δ values at zero field were used to obtain band offsets. (b) The average VB offsets [$\Delta E_{v\{av\}}$] over various temperatures, in order to compare with previously reported T-independent data.[2,7] The composition dependent $\Delta E_{v\{av\}}$ was obtained by a linear fit. Also shown are ΔE_v data adopted from Refs. 2 and 7.

IV. DISCUSSION

The T dependency of ΔE_v seems contradictory to the observation of T-independent ΔE_c reported by O'Shea *et al.*[2] However, our result is justifiable according to $\Delta E_g = \Delta E_c + \Delta E_v$, where the T variation of ΔE_g is accommodated by individual offset values. Comparison between experiments and calculations based on the ΔE_g^T data was carried out. This was evaluated by a percentage function $[\Delta E_g^T / \Delta E_g^{0K} - 1]$ as shown in Fig. 5(b). Two data sets of calculations based on TDIPS determined ΔE_v^T and the ΔE_c

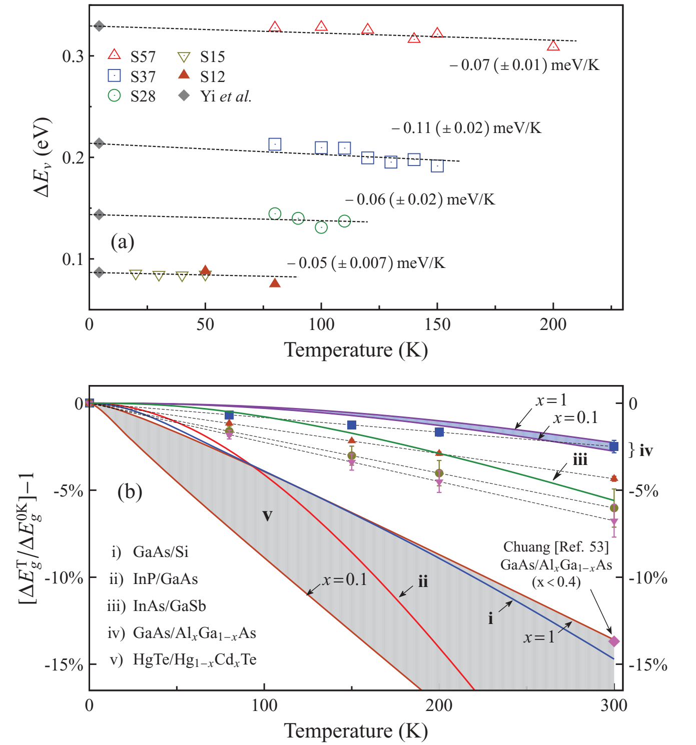

FIG. 5. (Color online) (a) Temperature-dependent VB offsets (scattered data) for different GaAs/$Al_xGa_{1-x}As$ samples. Shown are the temperature coefficients of ΔE_v obtained by linear fittings (dashed lines) and taking into account the data of Yi *et al.*[2] at 4.2 K. The T-dependent ΔE_v as a function of x was also obtained to be $\Delta E_v = (0.570 - 1.39 \times 10^{-4}\ T)x$ (eV). (b) Calculated $[\Delta E_g^T / \Delta E_g^{0K} - 1]$ as a function of temperature by using reported band-gap parameters:[6,7,13,53,54] i) GaAs/Si, ii) InP/GaAs, iii) InAs/GaSb, iv) GaAs/$Al_xGa_{1-x}As$, and v) HgTe/$Hg_{1-x}Cd_xTe$. The scattered data points are calculations using TDIPS determined ΔE_v^T and the ΔE_c data of O'Shea *et al.*.[2] The shaded areas correspond to heterojunctions with varied alloy fractions. The larger T dependence of band gaps implies more prominent T dependence in band offsets.

TABLE II. Comparison of ΔE_v from different reports for GaAs/$Al_xGa_{1-x}As$ heterojunctions. Previously reported offset data[2,7] are T independent. [BEES/BHES: ballistic electron/hole emission spectroscopy; JVT: current-voltage-temperature]

Reports	Methods	Temperature Range	ΔE_v (eV)
Yi *et al.* [2]	BEES/BHES	4.2 K	$(0.578 \pm 0.015)\,x$
Batey *et al.*[2]	JVT	80−300 K	$0.55\,x$
O'Shea *et al.* [7]	BEES	77 and 300 K	$0.53\,x$
Vurgaftman *et al.*[7]	–	300 K	$0.53\,x\ (x = 1)$
This work	TDIPS	20−200 K	$(0.570 - 1.39 \times 10^{-4}\ T)\,x$

data of O'Shea *et al.*,[2] and the band-gap parameters of $Al_xGa_{1-x}As$,[6,7] show a reasonable agreement, thus justifying our T-dependent results.

As it can be seen, the ΔE_v value of sample S57, which contains indirect-gap barriers ($x = 0.57$) is consistent with other direct-gap samples ($x < 0.42$). This is a consequence of the VB (of the emitter) to VB (of the barrier) emission, without the need of transitions across the band gap and the involving of X/L valleys. On the contrary, photoemission of electrons in n-type structures could be complicated by electron emission into the X/L valleys rather than Γ valley if an indirect-gap barrier is present. For this reason, TDIPS could have the advantage of characterizing type-II (staggered band alignment) and type-III (inverted electronic structure, e.g., HgTe/CdTe where the Γ_6 band of HgTe lies below the Γ_8 band) heterojunctions.

The parasitic charge in the barrier region of a heterojunction could be one of the sources of errors in the measurements, and usually needs to be determined in order to properly extract the band offsets, by techniques such as the capacitance-voltage (C-V) measurement. However, the space charges in the AlGaAs barriers of p-type structures are sufficiently small and can be safely excluded.[2,8] The most notable effect in the bias-dependent measurements is thus the MIF barrier lowering, which is well depicted by the agreement between the Δ values and the MIF fitting [see Fig. 4(a)]. To fit the MIF lowering, the selection of Δ data needs to exclude two bias regions. At biases around 0V, both forward and reverse photoemission currents coexist, which obscures the simple linear relationship of Δ-(Electric Field)$^{1/2}$. On the other hand, the quantum tunneling takes effect in the high field domain, which further reduces Δ. The data plotted in the inset of Fig. 4(a) focus on a moderate bias region and are thus accounted by the MIF lowering alone.

As for TDIPS measurements, degenerate doping can provide high photon absorption to enhance the yield and also prevents carrier freeze-out at very low temperatures. The $p^+ - i$ heterojunction with a doping density approaching or higher than the critical Mott transition density is somewhat similar to a metal-semiconductor system. On the other hand, doping-caused reduction in the band gap by BGR should be taken into account. Higher free-carrier density increases the many-body interactions between carriers, and between carriers and ionized impurities, which lowers the electron energy. From our results, BGR was properly handled based on the results of Jain *et al.*[43] under the rigid-band picture, where the VBs have a rigid upward shift.

Hole IPE was discussed by Helman *et al.*[46] on the basis of energy and transverse momentum conservation without considering the scattering effects. However, when the momentum conservation is explicitly required, the scattering effects should be taken into account. For elastic scattering, momentum conservation can be satisfied only if scattering events such as carrier-carrier, carrier-phonon scatterings, etc. are considered. For inelastic scattering (particularly in doped semiconductors), momentum conservation would not have to be obeyed. Therefore, it is infeasible to deduce the yield function by utilizing the momentum conservation when scattering events are involved. In our analysis, the quantum yield function has been formulated by taking into account the dominant photoexcitation and photoemission processes over the heterointerface as discussed in Sec. II. Since the momentum conservation is not explicitly considered in our model, both elastic and inelastic scattering processes can be allowed. Our analysis also neglects the influence of scattering on the determination of Δ, on the basis of an assumption that the energy dispersion of quantum yield is independent of scattering. Since TDIPS gives the results in agreement with previous band-offset reports [Fig. 4(b)] and the ΔE_g parameter [Fig. 5(b)], this assumption should be acceptable. Also, this assumption can be justified based on the analysis of Mooney *et al.*[47] on the scattering. In their analysis, each successive phonon collision gives isotropic momentum and lowers the magnitude by a factor. Therefore, the dependency of the yield function on the photon energy is actually not affected by scattering. Mooney *et al.* also showed[47] that the threshold remains the same under different scattering conditions. This indicates that the scattering effects can be neglected as far as the determination of photoemission thresholds is concerned.

The minute T variations of VB offsets in GaAs/AlGaAs heterojunctions are closely related to the temperature behavior of ΔE_g^T. In contrast to GaAs/AlGaAs, strong T-dependent ΔE_g^T can be found in InAs/GaSb and HgTe/$Hg_{1-x}Cd_xTe$[11] systems as shown in Fig. 5(b); both of which are of interest to fundamental research[48] as well as device applications.[13] The HgTe/$Hg_{1-x}Cd_xTe$ heterojunction has the largest temperature coefficient of ΔE_g^T. Several studies on its T-dependent band offsets have been reported.[11] InAs/GaSb has the type-II alignment (i.e., $\Delta E_g^T = |\Delta E_{c,0}^T - \Delta E_{v,0}^T|$) leading to much stronger T dependence in one of the band offsets over the another. Additionally, as shown in Fig. 5(b), more prominent T dependence could occur in the heterojunction family of large-lattice-mismatched systems such as InP/GaAs and

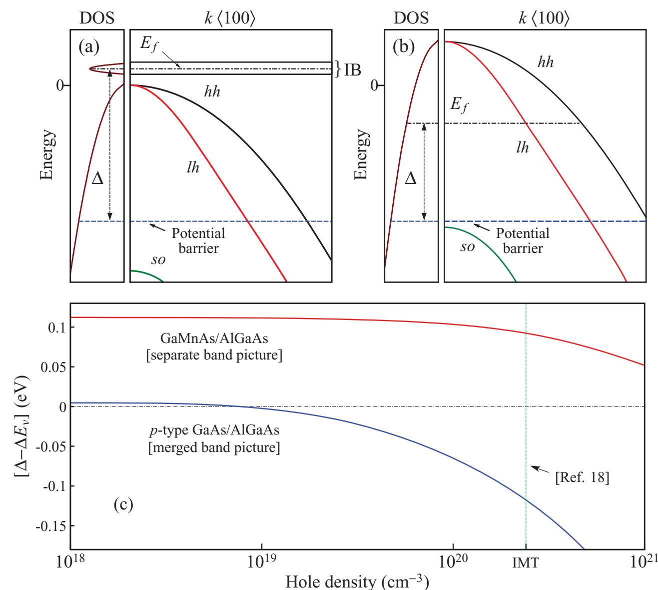

FIG. 6. (Color online) Schematics of DOS and VB structures of extrinsic semiconductors showing IB (a) separated from the VB and (b) merged with the VB. The VB of (b) is upward shifted rigidly by $\Delta_{\rm BGR}$. *hh*, *lh*, and *so* denote the heavy-hole, light-hole, and spin-orbit split-off bands, respectively. Δ is defined as the energy difference between E_f and the potential barrier. (c) Calculated $[\Delta - \Delta E_v]$ as a function of hole density for *p*-type (Ga,Mn)As/$Al_xGa_{1-x}As$ and GaAs/$Al_xGa_{1-x}As$ junctions. The Δ value of (Ga,Mn)As/$Al_xGa_{1-x}As$ is calculated by taking E_f data from Ohya *et al.*[19] and the Mn binding energy of 0.112 eV.[18] Indicated (dashed vertical line) corresponds to the IMT critical density.[18] The merged-band picture of (Ga,Mn)As should lead to a similar Δ variation to *p*-type GaAs.

III-V/Si. These structures have particular interests in developing hybrid photonic integrated circuits.[23]

Previous conclusions on the T-independent band offsets were mainly based on the assumption of similar T dependency of ΔE_g^T between the heterojunction constituents.[6] As shown in Fig. 5(b), this argument should not be universally valid. With the expansion of modern heterojunction family such as magnetic[49] and oxide[50] heterostructures, a careful inspection on the T dependence of band offsets would be needed. It was pointed out by Kroemer[8] that an understanding of offset variations on the ± 5 meV level is crucial even to device applications that can tolerate an accuracy better than ± 0.1 eV. The T-dependency nature very likely causes such a small variation and is thus more favorably considered as a universal characteristic, probably a necessity for the band-offset determination of some heterojunctions. A new strategy for designing devices is thus required accordingly.

As another application of the TDIPS method, a proposed measurement to identity the IB or VB conduction for (Ga,Mn)As is illustrated in Fig. 6. Typical clarification of the (Ga,Mn)As band structure is accomplished by distinguishing the IB-to-VB and VB-to-VB hole transitions,[22,51] which needs to track the optical properties of samples with varied Mn doping densities. In TDIPS measurements using heterojunctions such as (Ga,Mn)As/AlGaAs, E_f of (Ga,Mn)As can be obtained by determining the photoemission threshold. This process is similar to the analysis of sample S12a and S12b as described in Fig. 2(b), where a difference of 24.5 meV in E_f can be resolved. Figures 6(a) and 6(b) schematically show two band pictures of *p*-type (Ga,Mn)As with different Δ, associated with different E_f values. Because of the large binding energy of Mn (0.112 eV) and the very high hole density of (Ga,Mn)As, Δ of the IB conduction [Fig. 6(a)] is appreciably greater than that of the VB conduction [Fig. 6(b)]. Figure 6(c) plots Δ for both cases as a function of hole density, where nonmagnetic *p*-type GaAs was considered as an estimation. The merged-band picture of (Ga,Mn)As should resemble that of the *p*-type GaAs. An energy difference of 0.21 eV in Δ between two band pictures occurs at the IMT density,[18] and is nearly an order of magnitude greater than the *p*-type GaAs case [Fig. 2(b)]. This will enable TDIPS to be sufficient for studying (Ga,Mn)As.

V. CONCLUSION

In summary, studies on the band parameters of *p*-type heterojunctions were reported by using the VB-to-VB IPE measurements and the theoretical analysis. The significance of this paper includes (i) evidencing the universal characteristic of the T dependency in band offsets, (ii) disclosing the previously ignored T dependence of VB offsets for GaAs/$Al_xGa_{1-x}As$: $\Delta E_v = (0.570 - 1.39 \times 10^{-4}\ T)\, x$ (eV), and (iii) investigating the electronic structure of extrinsic semiconductors, such as clarifying the ambiguity in the band pictures of (Ga,Mn)As [IB or VB conduction].[52] Our conclusion on the band-offset T dependence is consistent with both theoretical and experimental studies. Our survey on the band-gap T behaviors confirms that particular attention should be given to the band-offset T dependency of several heterojunction systems with important application interests in the areas of optoelectronics and microelectronics.

ACKNOWLEDGMENTS

The authors gratefully acknowledge Dr. H. C. Liu for the sample processing, and Dr. K. K. Choi and Dr. P. Wijewarnasuriya for fruitful discussions. This work was supported in part by the US Army Research Office under Grant No. W911NF-12-2-0035 monitored by Dr. William W. Clark.

*uperera@gsu.edu

[1] H. Kroemer, Rev. Mod. Phys. **73**, 783 (2001); Z. I. Alferov, *ibid.* **73**, 767 (2001).

[2] J. Batey and S. L. Wright, J. Appl. Phys. **59**, 200 (1986); J. J. O'Shea, E. G. Brazel, M. E. Rubin, S. Bhargava, M. A. Chin, and V. Narayanamurti, Phys. Rev. B **56**, 2026 (1997); W. Yi,

V. Narayanamurti, H. Lu, M. A. Scarpulla, and A. C. Gossard, *ibid.* **81**, 235325 (2010).

[3]C. Coluzza, E. Tuncel, J.-L. Staehli, P. A. Baudat, G. Margaritondo, J. T. McKinley, A. Ueda, A. V. Barnes, R. G. Albridge, N. H. Tolk, D. Martin, F. Morier-Genoud, C. Dupuy, A. Rudra, and M. Ilegems, Phys. Rev. B **46**, 12834 (1992).

[4]C. Ghezzi, R. Magnanini, A. Parisini, L. Tarricone, E. Gombia, and M. Longo, Phys. Rev. B **77**, 125317 (2008).

[5]C. G. Van de Walle and R. M. Martin, Phys. Rev. B **35**, 8154 (1987); C. G. Van de Walle, *ibid.* **39**, 1871 (1989).

[6]S. Adachi, P. Capper, S. Kasap, and A. Willoughby, *Properties of semiconductor alloys: group-IV, III-V and II-VI semiconductors*, (Wiley, New York, 2009).

[7]I. Vurgaftman, J. R. Meyer, and L. R. Ram-Mohan, J. Appl. Phys. **89**, 5815 (2001).

[8]See, for example, H. Kroemer, Surf. Sci. **132**, 543 (1983); **174**, 299 (1986).

[9]A. Stroppa and M. Peressi, Phys. Rev. B **71**, 205303 (2005).

[10]W. R. L. Lambrecht and B. Segall, Phys. Rev. B **41**, 8353 (1990).

[11]For example, ΔE_v increasing with T was reported by D. H. Chow, J. O. McCaldin, A. R. Bonnefoi, T. C. McGill, I. K. Sou, and J. P. Faurie, Appl. Phys. Lett. **51**, 2230 (1987); In contrast, C. R. Becker, V. Latussek, A. Pfeuffer-Jeschke, G. Landwehr, and L. W. Molenkamp, Phys. Rev. B **62**, 10353 (2000) gave $d\Delta E_v/dT = -0.40 \pm 0.04$ meV/K.

[12]K. J. Malloy and J. A. V. Vechten, Appl. Phys. Lett. **54**, 937 (1989).

[13]J. P. Laurenti, J. Camassel, A. Bouhemadou, B. Toulouse, R. Legros, and A. Lusson, J. Appl. Phys. **67**, 6454 (1990).

[14]R. H. Fowler, Phys. Rev. **38**, 45 (1931).

[15]R. Nicolini, L. Vanzetti, G. Mula, G. Bratina, L. Sorba, A. Franciosi, M. Peressi, S. Baroni, R. Resta, A. Baldereschi, J. E. Angelo, and W. W. Gerberich, Phys. Rev. Lett. **72**, 294 (1994).

[16]Y. Zhang and S. Das Sarma, Phys. Rev. B **72**, 125303 (2005).

[17]J. Tauc, Science **158**, 1543 (1967).

[18]B. C. Chapler, R. C. Myers, S. Mack, A. Frenzel, B. C. Pursley, K. S. Burch, E. J. Singley, A. M. Dattelbaum, N. Samarth, D. D. Awschalom, and D. N. Basov, Phys. Rev. B **84**, 081203 (2011).

[19]S. Ohya, K. Takata, and M. Tanaka, Nature Phys. **7**, 342 (2011).

[20]M. Dobrowolska, K. Tivakornsasithorn, X. Liu, J. K. Furdyna, M. Berciu, K. M. Yu, and W. Walukiewicz, Nature Mater. **11**, 444 (2012).

[21]T. Dietl, H. Ohno, F. Matsukura, J. Cibert, and D. Ferrand, Science **287**, 1019 (2000).

[22]T. Jungwirth, P. Horodyská, N. Tesařová, P. Němec, J. Šubrt, P. Malý, P. Kužel, C. Kadlec, J. Mašek, I. Němec, M. Orlita, V. Novák, K. Olejník, Z. Šobáň, P. Vašek, P. Svoboda, and J. Sinova, Phys. Rev. Lett. **105**, 227201 (2010).

[23]K. Tanabe, K. Watanabe, and Y. Arakawa, Sci. Rep. **2**, 1 (2012).

[24]A. Braunstein, M. Braunstein, G. S. Picus, and C. A. Mead, Phys. Rev. Lett. **14**, 219 (1965).

[25]A. Prem and V. V. Kresin, Phys. Rev. A **85**, 025201 (2012).

[26]F. Williams and A. J. Nozik, Nature (London) **312**, 21 (1984).

[27]M. Cinchetti, K. Heimer, J.-P. Wüstenberg, O. Andreyev, M. Bauer, S. Lach, C. Ziegler, Y. Gao, and M. Aeschlimann, Nature Mater. **8**, 115 (2009).

[28]W. Wang, G. Lüpke, M. D. Ventra, S. T. Pantelides, J. M. Gilligan, N. H. Tolk, I. C. Kizilyalli, P. K. Roy, G. Margaritondo, and G. Lucovsky, Phys. Rev. Lett. **81**, 4224 (1998).

[29]S. M. Sze and K. K. Ng, *Physics of Semiconductor Devices* (Wiley, New York, 2007), Chap. 3.

[30]C. Caroli, J. S. Helman, and F. S. Sinencio, Phys. Rev. B **11**, 980 (1975).

[31]E. O. Kane, Phys. Rev. **127**, 131 (1962).

[32]W. Seidel, O. Krebs, P. Voisin, J. C. Harmand, F. Aristone, and J. F. Palmier, Phys. Rev. B **55**, 2274 (1997).

[33]V. V. Afanas'ev and A. Stesmans, J. Appl. Phys. **102**, 081301 (2007).

[34]Y. F. Lao, P. K. D. D. P. Pitigala, A. G. U. Perera, H. C. Liu, M. Buchanan, Z. R. Wasilewski, K. K. Choi, and P. Wijewarnasuriya, Appl. Phys. Lett. **97**, 091104 (2010).

[35]R. Williams, *Injection Phenomena*, edited by R. Willardson and A. Beer, Semiconductors and Semimetals (Academic Press, New York, 1970), Chap. 2.

[36]A. M. Goodman, Phys. Rev. **152**, 785 (1966).

[37]R. J. Powell, J. Appl. Phys. **41**, 2424 (1970).

[38]E. O. Kane, Phys. Rev. **131**, 79 (1963).

[39]T. Nakamura, T. Takahashi, and S. Adachi, Phys. Rev. B **81**, 125324 (2010).

[40]I.-S. Chen, T. N. Jackson, and C. R. Wronski, J. Appl. Phys. **79**, 8470 (1996).

[41]T. B. Bahder, Phys. Rev. B **41**, 11992 (1990).

[42]H. Neumann, B. Jacobs, and W. Hörig, Crys. Res. Technol. **25**, 343 (1990).

[43]S. Jain and D. Roulston, Solid-State Electron. **34**, 453 (1991).

[44]D. V. Geppert, J. Appl. Phys. **34**, 490 (1963).

[45]E. Kioupakis, P. Rinke, A. Schleife, F. Bechstedt, and C. G. Van de Walle, Phys. Rev. B **81**, 241201 (2010).

[46]J. S. Helman and F. Sánchez-Sinencio, Phys. Rev. B **7**, 3702 (1973).

[47]J. M. Mooney and J. Silverman, IEEE Trans. Electron Devices **32**, 33 (1985).

[48]C. Liu, T. L. Hughes, X.-L. Qi, K. Wang, and S.-C. Zhang, Phys. Rev. Lett. **100**, 236601 (2008).

[49]Y. Ohno, D. K. Young, B. Beschoten, F. Matsukura, H. Ohno, and D. D. Awschalom, Nature (London) **402**, 790 (1999).

[50]H. Y. Hwang, Y. Iwasa, M. Kawasaki, B. Keimer, N. Nagaosa, and Y. Tokura, Nature Mater. **11**, 103 (2012).

[51]K. S. Burch, D. B. Shrekenhamer, E. J. Singley, J. Stephens, B. L. Sheu, R. K. Kawakami, P. Schiffer, N. Samarth, D. D. Awschalom, and D. N. Basov, Phys. Rev. Lett. **97**, 087208 (2006).

[52]N. Samarth, Nat. Mater. **11**, 360 (2012).

[53]S. L. Chuang, *Physics of Optoelectronic Devices* (Wiley, New York, 1995).

[54]K. P. O'Donnell and X. Chen, Appl. Phys. Lett. **58**, 2924 (1991).